Transactions on Additive Manufacturing Meets Medicine
Trans. AMMM, 2026, Vol. 8, No 1, Article ID 2757, 7 Pages

Infinite Science Publishing

Original Research Article

A patient-derived 3D-printed silicone model for studying pharyngeal collapse and flow limitation in obstructive sleep apnea

A. Ibbeken[1*], C. Hagen[1,2], F. Zell[1], U. Kirstein[3], A. Frydrychowicz[3], A. Steffen[4], and T. M. Buzug[1,2]

[1] *Institute of Medical Engineering, Universität zu Lübeck, Lübeck, Germany*
[2] *Fraunhofer Research Institution for Individualized Medical Technology and Engineering IMTE, Lübeck, Germany*
[3] *Department of Radiology and Nuclear Medicine, Universitätsklinikum Schleswig-Holstein, Lübeck, Germany*
[4] *Department of Ear, Nose and Throat Medicine, Universitätsklinikum Schleswig-Holstein, Lübeck, Germany*
[*] *Corresponding author, email: al.ibbeken@uni-luebeck.de*

Received March 26, 2026; **Accepted** April 24, 2026; **Published online** June 14, 2026

© 2026 Alina Ibbeken; licensee Infinite Science Publishing
This is an Open Access abstract distributed under the terms of the Creative Commons Attribution License, which permits unrestricted use, distribution, and reproduction in any medium, provided the original work is properly cited (http://creativecommons.org/licenses/by/4.0).

Abstract: Obstructive sleep apnea (OSA) is caused by dynamic collapse of the upper airway during inspiration; realistic upper airway phantoms that combine imaging and pressure-flow measurements are needed to study collapse mechanics and evaluate therapies. The objective of this study is to fabricate and validate an additively manufactured, patient-specific silicone upper-airway phantom that reproduces reversible, reproducible pharyngeal collapse and to quantify its deformation with computer tomography (CT) imaging and its pressure-flow behavior under controlled inspiratory suction. The airway lumen was segmented from a clinical magnetic resonance imaging (MRI) dataset and converted into a two-part casting mold. A rigid outer shell and a water-soluble airway core were 3D-printed; regions corresponding to soft palate, tongue and lateral walls were cast in compliant silicone. The assembled phantom was mounted in a flow rig and measured with CT imaging in baseline, moderate flow (~5 l/min) and collapsed states. Pressure and flow were recorded in separate, identically controlled runs to derive airway resistance and identify collapse thresholds. CT showed focal, reproducible collapse at the soft palate and tongue base with minimal cross-sectional area reductions of 91 % and 97 %, respectively; flexible airway volume decreased from 8.0 cm^3 (baseline) to 3.92 cm^3 (collapsed), a 51.6 % reduction. Collapse produced flow limitation (flow oscillating ≈ 0-1 l/min) and a characteristic pressure–flow loop; the critical closing pressure immediately prior to collapse was ≈ −2.4 mbar. All deformation and aerodynamic signatures were reversible and reproducible across repeats. The patient-specific silicone phantom replicates key mechanical features of a collapsible pharynx and provides a controlled, image-verified platform for mechanistic studies and preclinical testing of anatomical interventions.

I. Introduction

Obstructive sleep apnea (OSA) is a common disorder in which the collapsible pharynx intermittently narrows or closes during sleep, causing airflow limitation, oxygen desaturation, sleep fragmentation and increased cardiometabolic risk [1, 2]. The mechanical behavior of the upper airway - its geometry, tissue compliance and the interaction with inspiratory suction - determines where and when collapse occurs. Understanding these structure-function relationships is essential for improving diagnosis and for tailoring anatomical interventions such as mandibular advancement devices.

Negative-effort dependence (NED) - a principal functional characteristic of OSA - is an important but comparatively under-investigated mechanical consequence of these interactions [3, 4, 5]. NED denotes the paradoxical situation in which increasing inspiratory effort produces no further increase in airflow (flow limitation) and may even reduce flow once a critical level of negative pharyngeal pressure is reached (Fig 1). Mechanistically, this arises when compliant pharyngeal walls at a focal weak point (for example the soft palate or tongue base) contact under negative transmural pressure, forming a pressure-controlled occlusive segment that decouples downstream driving pressure from the delivered flow [5, 6, 7].

Clinically, NED is a useful functional readout of pharyngeal collapsibility; experimentally, reproducing NED in vitro requires anatomically accurate models whose soft-tissue mechanics can be tuned and whose aerodynamics can be measured directly. In-vitro patient-

specific phantoms that reproduce realistic soft-tissue mechanics meet these needs and therefore provide a controlled platform to study pharyngeal collapse. Prior physical models have often used simplified geometries, non-physiologic materials, or lacked image-based validation and simultaneous aerodynamic measurement, limiting their fidelity and reproducibility [9, 10, 11, 12, 13]. Additive manufacturing combined with compliant silicone casting enables fabrication of anatomically accurate, reproducible, and radiopaque-compatible phantoms that can be examined with computed tomography (CT) imaging and pressure-flow measurements.

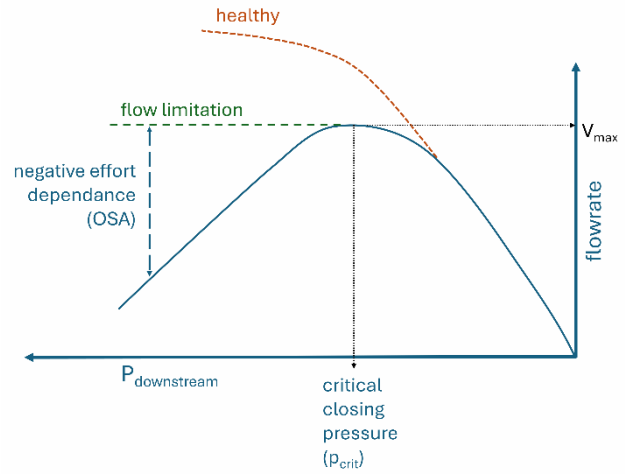


Figure 1: Schematic pressure–flow relationship in the collapsible pharynx, comparing a healthy airway with an obstructive sleep apnea (OSA) airway. In a healthy airway, progressively more negative pharyngeal pressure (increasing inspiratory effort) yields a proportional increase in inspiratory flow. In a collapsible OSA airway, however, once downstream pressure falls below a critical closing pressure (P_{crit}) and flow limitation occurs: further increases in negative pressure fail to increase flow and can even reduce it (negative-effort dependence, NED). Flow limitation and NED reflect elevated pharyngeal collapsibility and are central features of sleep-disordered breathing [Image adapted from 8].

The aim of this study was to develop and validate an additively manufactured, patient-specific silicone upper-airway phantom that exhibits reproducible, reversible pharyngeal collapse. Specifically, we (i) fabricated a hybrid rigid–compliant model from a magnetic resonance imaging (MRI) dataset, (ii) quantified geometric deformation of the airway under controlled inspiratory suction using computed tomography imaging (CT), and (iii) characterized the corresponding pressure–flow behavior and airway resistance during collapse and recovery. We hypothesized that the phantom would reproduce focal, repeatable collapse at clinically relevant sites and display pressure-flow behaviour - including NED - qualitatively comparable to OSA physiology.

II. Material and methods

The following sections provide a systematic, step-by-step account of the fabrication and characterization of the patient-specific phantom. The phantom was constructed according to the procedure described in Ibbeken et al. [14].

II.I. Model construction

The patient-specific upper airway geometry was derived from clinical MR image data (3T MR system, Ingenia, Philips, Amsterdam, Netherlands; MR parameters: TR = 700 ms, TE = 35 ms, flip angle = 90°, pixel spacing = 0.58 x 0.58 mm^2, slice thickness = 1 mm) of a patient with obstructive sleep apnea (apnea-hypopnea-index: 27, oxygen desaturation index: 15, BMI: 26, age: 58, sex: female) (Fig. 2). The nasopharynx, oropharynx and laryngopharynx were segmented semi-atuomatically by clinical experts from the image set using ITK-SNAP (www.itksnap.org) [15] and exported as a surface mesh. The nasal and oral cavities were excluded; accordingly, the model extends from the choanae (nasal–nasopharyngeal transition) to the laryngeal inlet and includes a few centimeters of the proximal trachea.

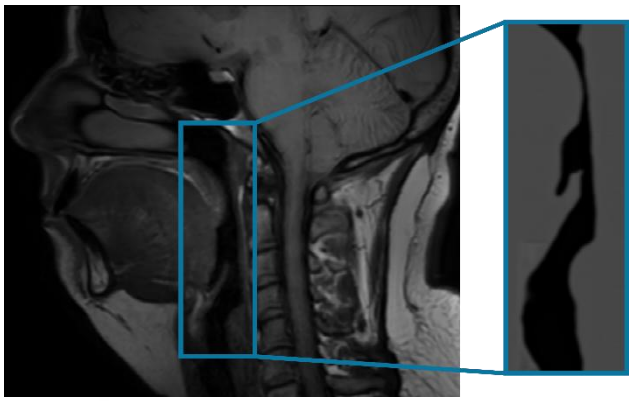


Figure 2: Left: magnetic resonance image of the upper airway from a patient with OSA, used to segment the airway lumen (nasopharynx, oropharynx and laryngopharynx; nasal and oral cavity excluded) for model generation. Right: CT scan of the assembled silicone airway phantom after 3D printing and molding.

The digital airway surface was smoothed (smoothing scale 10, smoothing type: shape preserving) and reduced to 30.000 triangles in MeshMixer (Autodesk, Mill Valley, California, USA) for further processing with SolidWorks (Dassault Systèmes, Vélizy-Villacoublay, France) to produce a two-part casting mold: a rigid outer shell representing the non-compliant surrounding tissues (trachea and other hard anatomical boundaries) and a removable inner core representing the airway lumen. The outer shell was printed in a rigid polymer using a multijet-printer (J850 (Stratasys, Minnesota, USA), material: Vero Clear). The airway core and selected parts of the mold were printed in a water-soluble material with a material extrusion printer (Ultimaker 3, Ultimaker, Gendermalsen, Netherlands), material: FormFutura AquaSolve PVA) to allow later dissolution. Regions of the upper airway that correspond to soft tissue (tongue, soft palate, lateral pharyngeal walls) were geometrically simplified in form of a cylindrical shape and were reproduced with a flexible silicone cast. A two-step casting procedure was used: the 3D printed mold was assembled with the integrated water-soluble airway geometry (Fig. 3), silicone was poured into

the casting mold representing soft tissue components, and was cured according to the manufacturer's instructions. After curing, the water-soluble parts of the mold (airway lumen and upper outer shell) were dissolved in water, leaving a compliant airway enclosed in flexible silicone surrounding and based on the rigid outer shell. The two-component silicone formulation (Sylgard 527 Silicone Dielectric Gel, Dow Corning, Midland, Michigan, USA) was chosen to match the elastic behavior of upper airway soft tissues [16, 17] using a mixing ratio of 1:1 to gain a Youngs modulus of 5 kPa [18]. The posterior pharyngeal wall of the airway was manufactured with integrated pressure ports (small bore holes) to accept pressure transducers for intrapharyngeal pressure measurements.

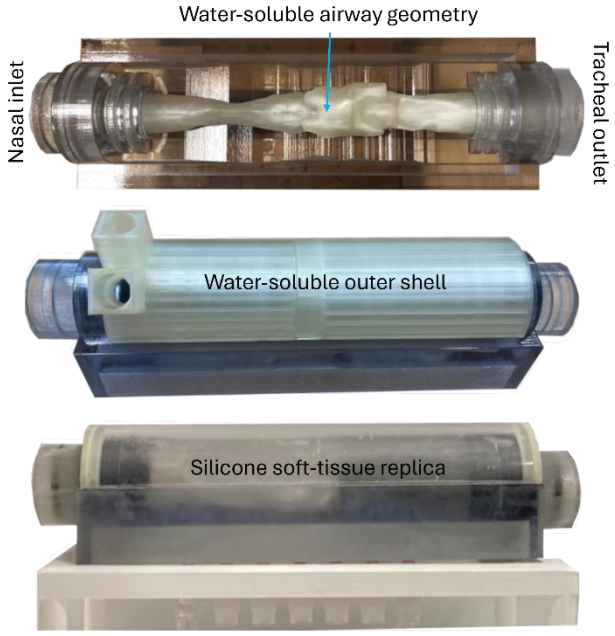


Figure 3: Fabrication steps of the airway phantom (images arranged top to bottom). (A) Solid base of the model with the water-soluble printed airway template inserted into the casting assembly. (B) Assembled mold showing the outer water-soluble components with integrated inlet and outlet ports for silicone casting. (C) Final silicone airway phantom after dissolving the water-soluble components - a flexible silicone sleeve surrounds the hollow airway lumen.

II.II. Experimental setup

The airway phantom was mounted in a flow setup designed to reproduce inspiratory suction. One meter straight inlet and outlet tubes were connected to the nasal and tracheal ends of the model to promote laminar flow development prior to the geometry. Airflow was driven by a custom-made flow pump operating in suction mode to mimic inhalation. Instantaneous volumetric flow was measured with a mass flow meter from Sensirion (SFM 3000, Sensirion, Stäfa, Switzerland). Static pressure was recorded with a pressure transducer (AMS 5915, Analog Microelectronics GmbH, Mainz, Germany) at the downstream (tracheal outlet) position. A schematic of the flow setup is presented in Figure 4.

Inspiratory suction was generated by a downstream, voltage-driven centrifugal vacuum blower (compact fan with universal motor; Electrolux AEG, part no. 4055337127), producing sub-atmospheric pressure at the tracheal outlet. The blower was powered by an adjustable bench supply and operated open-loop; volumetric flow was set by the applied voltage. To induce collapse reproducibly, we applied a step actuation: the power supply was preset to its target voltage and then switched on, resulting in a rapid rise in flow. Flow and pressure were monitored continuously (SFM3000; AMS5915). For CT imaging in the collapsed state, acquisition was initiated once the flow-limited condition stabilized.

Because actuation was step-like, gradients were quantified from the recorded flow signal. The 10-90% rise time was 0.25 ± 0.01 s (mean ± SD, n = 6), corresponding to a peak flow of 7.85 ± 0.07 l/min. This rise is faster than typical resting human inspiratory ramps (peak flows ~10-20 l/min reached over ~1-2 s), by design, to trigger collapse promptly and minimize intermediate, partially deformed states.

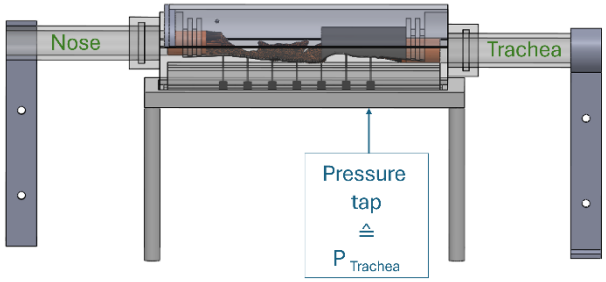


Figure 4: Schematic of the experimental upper-airway model showing the integrated airway geometry, inlet and outlet tubing, and pressure taps drilled into the posterior pharyngeal wall for transducer measurements. The model is connected to a ventilation pump and flow sensor to simulate inspiratory flow and provoke collapses in the flexible silicone (soft-tissue) region, while rigid 3D-printed segments represent non-collapsible anatomy.

II.III. CT deformation measurements

To quantify airway deformation, the entire flow rig including the mounted phantom was transferred to the CT scanner. CT imaging was performed with a Siemens CT scanner (Somatom Definition AS+, Siemens Healthineers, Erlangen, Germany) with a voxel spacing of 0.16 x 0.16 x 0.3 mm^3 and a peak tube voltage of 120 kVp. Three imaging states were recorded in each experimental run: baseline (no flow), deformed due to flow and recovered (flow reduced and airway returned to baseline geometry). Two states of deformation due to flow were recorded: beginning contraction of the phantom according to a flow of 5 l/min and a full collapse of the phantom leading to flow limitation (flow oscillates around 0-1 l/min). For each CT condition (baseline, moderate flow, collapsed) the pump was set to the target flow and allowed to reach steady state prior to imaging.

Infinite Science Publishing

II.IV. Image processing and deformation analysis

CT volumes were segmented to extract the airway lumen for each imaging state using semi-automatic thresholding and manual editing in ITK-SNAP. Cross-sectional areas were computed on planes orthogonal to the airway centerline to quantify local collapses. Area profiles from the different imaging states were graphically overlaid for direct, comparative visualization. We also computed, for each airway state, the minimum cross-sectional area for the two sides of collapse (soft palate and base of tongue), the area reduction (degree of stenosis)-defined as the ratio of area at the side of collapse of the collapsed airway to the undeformed airway-and the airway volume of the flexible airway area.

II.V. Pressure-flow analysis

Pressure and flow recordings were acquired separately from the CT scans. CT imaging and aerodynamic measurements were performed in separate experimental runs but using identical pump settings and flow profiles. Within the aerodynamic recordings, pressure sensors were synchronized with the flow sensor, and airway resistance was computed from simultaneous measurements of the pressure drop $\Delta P = P_{upstream} - P_{downstream}$ and volumetric flow Q using the definition $R = \Delta P/Q$. In the experiments $P_{upstream}$ was taken equal to atmospheric pressure (P_{atm}), so $\Delta P = P_{atm} - P_{downstream}$. The pressure–flow relationship during progressive suction and subsequent recovery was plotted and the collapse event identified by the onset of flow limitation with negative-effort dependence.

III. Results and discussion

The aim of these experiments was to verify that the 3D-printed, silicone-based phantom reproduces realistic, reversible upper-airway collapse that can be detected both by CT imaging and by pressure/flow measurements. In the following we summarize and interpret the CT deformation data and the pressure–flow measurements. The principal finding is that the silicone airway phantom exhibits reversible, reproducible pharyngeal collapse: the minimal lumen area decreased markedly with increasing inspiratory suction and the model entered a flow-limited state with negative effort dependence. These geometric changes occurred in parallel with a substantial increase in the pressure drop ($\Delta P = P_{atm} - P_{downstream}$) and with a rise in calculated airway resistance. Below we present the imaging results first and then the pressure/flow analysis.

III.I. CT deformation measurements

We acquired CT volumes in three conditions: baseline (no flow), during moderate inspiratory flow (~5 l/min), and in a collapsed state induced by progressively increasing suction. Longitudinal CT slices (Fig. 5) show that at ~5 l/min the airway geometry is largely unchanged, whereas under high suction the lumen undergoes pronounced, reproducible collapse. Collapse was concentrated at two anatomical sites - the soft palate and the tongue base - and in addition a direct comparison of the surface meshes (Fig. 6) reveals a marked reduction in cross-sectional area throughout the oropharynx as well.

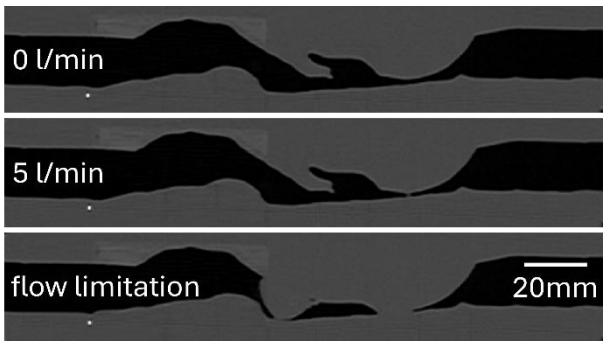


Figure 5: Sagittal (longitudinal) view of the airway CT images. Top: no flow (baseline); middle: moderate inspiratory flow (~5 l/min); bottom: flow limitation with near-complete collapse (flow ≈ 0 l/min) at two anatomical landmarks: the soft palate and the base of the tongue.

Quantitative extraction of lumen geometry was performed by computing transverse cross-sectional areas orthogonal to the airway centerline. From the cross-sectional area profiles, we derived the key geometric parameters used to characterize airway state shown in Table 1.

A_{min} decreased progressively from baseline to the flow-limited state leading to a total area reduction of 91 % in the area of the soft palate and of 97 % in the area of the base of the tongue. The airway volume of the flexible airway area, computed by integrating the cross-sectional areas, reduces with increasing inspiratory flow from 8.09 cm^3 to a minimum of 3.92 cm^3 in the flow-limited state leading to a total volume reduction of 51.6 %.

Table 1: Key parameters for airway characterization.

	A_{min} soft palate (mm^2) / area reduction	A_{min} base of tongue (mm^2) / area reduction	Flexible airway volume (cm^3)
0 l/min	17.5 / 0	86.6 / 0	8.09
5 l/min	12.3 / 0.30	78.2 / 0.10	7.60
Flow lim.	1.5 / 0.91	2.4 / 0.97	3.92

The area-profiles are plotted in Fig. 7 for four states: initial baseline (0-l/min), moderate flow (~5 l/min), flow limitation (collapsed state), and a final null measurement acquired after the experiment to assess elastic recovery. These profiles show two distinct, reproducible minima in cross-sectional area that deepen with increasing inspiratory demand, corresponding to the two collapsed levels seen in the meshes (Fig. 6).

Infinite Science Publishing

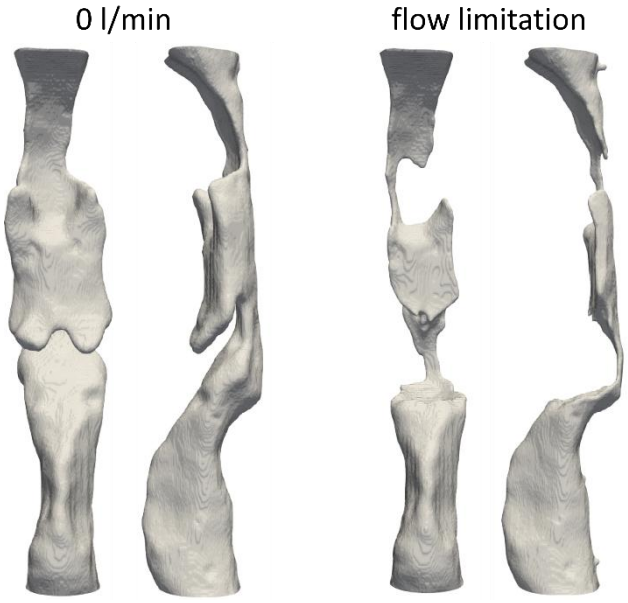


Figure 6: Comparison of airway surface meshes reconstructed from CT for the patient-specific model at baseline (0 l/min, undeformed) and during flow-limitation (collapsed). Sagittal and coronal views show focal luminal collapse at the soft palate and at the tongue base.

A final reference CT acquired after the loading sequence returned to a geometry that matched the initial baseline within the limits of image segmentation, demonstrating elastic, reversible behavior and good reproducibility of the measured deformation patterns. The flow-limitation experiment itself was repeated twice; the two collapsed area profiles overlapped closely (Fig. 7), confirming reproducibility of the collapse location and magnitude.

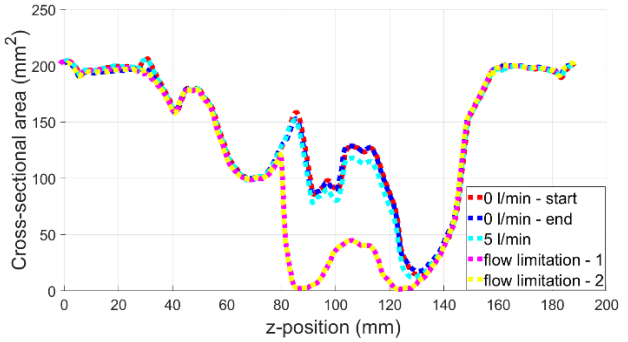


Figure 7: Plot of calculated transverse cross-sectional airway area versus axial position along the airway (z = 0 mm defined at the tracheal outlet, progressing to z ≈ 180 mm at the nasal inlet). Traces show the airway at baseline (0 l/min), during moderate inspiratory flow (~5 l/min), the flow-limited (collapsed) state, and a final null (post-test) measurement to assess elastic recovery. The flow-limitation measurement was repeated twice (two collapsed-state traces) to demonstrate reproducibility of the collapse pattern. Focal area reductions occur at the soft-palate and tongue-base regions.

Together, the mesh visualizations (Fig. 6) and the cross-sectional area plots (Fig. 7), supported by the cross-sectional slices shown in Fig. 5, demonstrate that collapse in this patient-specific silicone phantom is focal (soft palate and tongue base), reproducible, and quantifiable using the described geometric metrics.

III.II. Pressure-flow analysis

The time-series traces (Fig. 8) show the characteristic sequence of events during progressive inspiratory suction: as the pump is ramped up, tracheal pressure becomes increasingly negative and inspiratory flow rises. Throughout this phase, the computed resistance increases gradually, reflecting progressive luminal narrowing visible on the CT scans. When the negative pressure reaches a critical threshold, the pharyngeal lumen collapses. Collapse is identified by an abrupt fall in flow (to near 0-1 L/min in these experiments). The flow pattern during collapse shows extensive oscillations like a snoring pattern during OSA. Following a reduction in pump suction, tracheal pressure returns toward atmospheric, the airway reopens, flow recovers, and resistance returns toward its baseline value; this recovery is reproducible across repeated runs.

The pressure-flow diagram (Fig. 9) illustrates the collapse-recovery cycle: during the rising phase (increasing negative pressure from 0 mbar to approx. -2.5 mbar, blue graph) flow initially follows the expected increase until a plateau is reached and then rapidly drops at the point of collapse. The collapse phase therefore demonstrates negative-effort dependence (increasing inspiratory effort leads to a reduced respiratory flow), a characteristic feature of obstructive sleep apnea physiology. The recovery phase (red graph) follows a different trajectory shifted to slightly higher pressures, producing a loop that indicates hysteresis between collapse and reopening: a possible explanation would be the adhesion between the collapsed silicone walls leading to an increase of the required pressure for airway reopening relative to the collapse threshold.

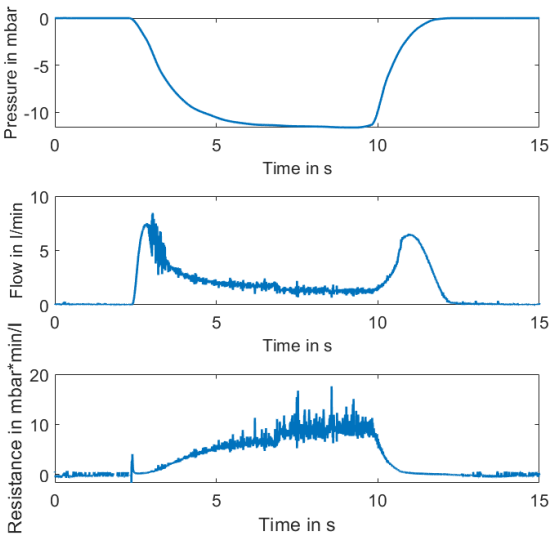


Figure 8: Recorded traces of flow, pressure, and the derived airway resistance. As the airway lumen progressively narrows, the resistance rises steadily and eventually plateaus at approximately 10 mbar·min/l. This pattern reflects progressive flow limitation: once a critical negative pressure is reached, further increase in driving suction produces little or no increase in flow while resistance remains elevated.

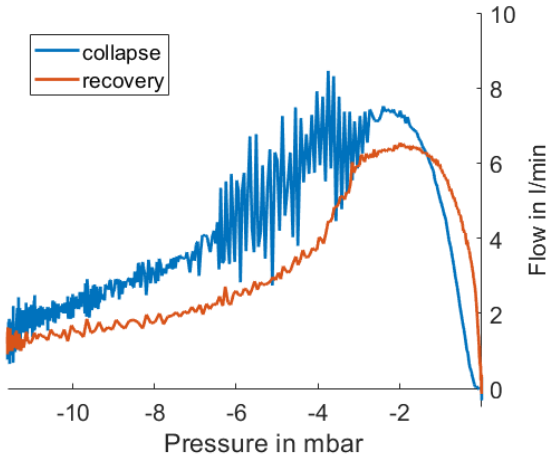


Figure 9: The pressure–flow diagram characterizes both the dynamic collapse of the pharynx and its subsequent recovery to the undeformed baseline. In the collapse phase (blue graph), progressive increases in negative pharyngeal pressure (i.e., increasing inspiratory effort) cause flow to rise initially until a critical pressure of approximately -2.4 mbar is reached, corresponding to a peak flow of about 7.84 l/min (flow limitation). Once the pressure falls beyond this critical value, the pharyngeal walls abruptly collapse, and the flow drops to roughly 0-1 l/min while the pressure continues to fall to about -11.5 mbar. This sudden reduction in flow despite increasing effort reproduces the negative effort dependence commonly seen in OSA patients. In the recovery phase (red graph), after the driving pump is turned off the negative pressure relaxes towards atmospheric pressure, the airway reopens, and a transient residual flow is observed until the system returns to zero flow.

III.III. Interpretation and relevance

These pressure-flow dynamics confirm that the patient-specific silicone phantom reproduces the key mechanical behaviors of a collapsible pharynx: progressive narrowing with increasing negative pressure, an abrupt, reproducible collapse at a definable critical pressure, and reversible reopening on pressure relief. The shape of the pressure–flow loop is qualitatively similar to clinical descriptions of flow limitation and negative-effort dependence in OSA patients [5, 19]. Expressed in the conventional units used clinically (-2.4 mbar ≈ -2.45 cmH2O), the measured P_{crit} falls within the reported range of in vivo measurements summarized in a review by Kazemeini et al. [20] (see Table 1), supporting the physiological accuracy of the phantom.

III.IV. Limitations and implications

Several limitations should be noted. First, measurements were performed on a single patient-specific geometry; generalization requires testing additional anatomies. Second, although the chosen silicone approximates tissue stiffness, it does not replicate all viscoelastic properties of living soft tissues; this could affect dynamic collapse timing and hysteresis. Third, CT finite resolution and segmentation uncertainty limit precision for small area changes. Finally, the experimental boundary conditions (long rigid inlet/outlet tubes, steady suction profile with constant flow) simplify in vivo breathing variability and neuromuscular influences.

Despite these limitations, the model provides a reproducible, image-verified testbed that integrates airway geometry with pressure-flow measurements. It is therefore well suited for controlled comparative studies and investigations of collapse mechanics and flow-structure interaction of OSA.

IV. Conclusions

Combined CT imaging and pressure–flow measurements demonstrate that the patient-specific, additively manufactured silicone phantom reliably reproduces focal, reversible pharyngeal collapse and directly links geometric narrowing to severe flow limitation. The model's repeatable, imaging-based measurements - cross-sectional area, volume change, critical closing pressure, and resistance - allow for quantitative correlation of airway geometry and aerodynamic performance. Because collapse is both repeatable and reversible in this testbed, it is well suited for controlled, comparative testing of therapeutic approaches.

As a next step, we will produce two additional pharyngeal models from the same patient anatomy incorporating a mandibular advancement device (MAD) at two clinically relevant degrees of protrusion (moderate and maximal comfortable advancement). These will be fabricated following the same workflow and tested with identical CT deformation scans and simultaneous pressure/flow recordings. We hypothesize that mandibular advancement will reduce collapsibility - manifest as smaller deformations, reduced pressure drop and increased critical closing pressure - and that the magnitude of these effects will scale with protrusion. Future work should expand to multiple patient anatomies, incorporate variable jaw positions and simulated neuromuscular tone.

Acknowledgments

This work has been funded by the German Federal Ministry of Education and Research (BMBF Grant Number 13GW0276B).

Author's statement

Authors state no conflict of interest. Informed consent: Informed consent has been obtained from all individuals included in this study. Ethical approval: All procedures performed in studies involving human participants were in accordance with the ethical standards of the institution or practice at which the studies were conducted. The local ethics committee (AZ 19–021) approved this prospective study (I-SLEEP).

References

[1] A. S. Jordan, D. G. McSharry, A. Malhotra, Adult obstructive sleep apnoea. in Lancet vol. 383,9918, 2014, pp. 736-747.

[2] J. A. Dempsey, S. C. Veasey, B. J. Morgan, C. P. O'Donnell, Pathophysiology of sleep apnea, in Physiological reviews vol. 90,1, 2010, pp.47-112.

[3] J. P. Butler, R. L. Owens, A.Malhotra, A. Wellman, CrossTalk opposing view: the human upper airway during sleep does not behave like a Starling resistor, The Journal of physiology vol. 591,9, 2013, pp. 2233-2234.

[4] R. L. Owens, B. A. Edwards, S.A. Sands, J.P. Butler, D.J. Eckert, D.P. White. A. Malhotra, A. Wellman, The classical Starling resistor model often does not predict inspiratory airflow patterns in the human upper airway, Journal of applied physiology vol. 116,8,2014, pp. 1105-1112.

[5] A. Wellman, P.R. Genta, R.L. Owens, B.A. Edwards, S.A. Sands, S. H. Loring, D.P. White, A.C. Jackson, O. F. Pederson, J. P. Butler, Test of the Starling resistor model in the human upper airway during sleep, Journal of applied physiology vol.117,12, 2014, pp. 1478-1485.

[6] A. R. Schwartz, P. L. Smith, CrossTalk proposal: The human upper airway does behave like a Starling resistor during sleep, The Journal of physiology vol. 591,9,2013, pp.2229-2232.

[7] A.R. Gold, A.R. Schwartz, The pharyngeal critical pressure. The whys and hows of using nasal continuous positive airway pressure diagnostically, Chest vol. 110,4 ,1996, pp. 1077-1088.

[8] T. B. Le., M.G. Moghaddam, B.T. Woodson, G.J.M. Garcia, Airflow limitation in a collapsible model of the human pharynx: physical mechanisms studied with fluid-structure interaction simulations and experiments, Physiological reports vol. 7.10, 2019, pp. e14099.

[9] A.I. Katz, Y. Chen, A.h. Moreno, Flow through a Collapsible Tube: Experimental Analysis and Mathematical Model, Biophysical Journal vol. 9.10, 1969, pp.11261-1279.

[10] J. Amatoury, K. Kairaitis, J.R. Wheatley, L.E. Bilston, T.C. Amis, Onset of airflow limitation in a collapsible tube model: impact of surrounding pressure, longitudinal strain, and wall folding geometry, Journal of Applied Physiology vol.109.5, 2010, pp. 1467-1475.

[11] M. Al-Abed, P. Antich, D. E. Watenpaugh, K. Behbehani, Phantom study evaluating detection of simulated upper airway occlusion using piezoelectric ultrasound transducers, Computers in Biology and Medicine vol. 89,10,2017, pp.325-336.

[12] W. Yan, S. Zhang, Y. Liu, G. Li, Numerical simulations and experimental measurements on flow features in a patient-specific upper airway model with obstructive sleep apnea, Proceedings of the Institution of Mechanical Engineers, Part C: Journal of Mechanical Engineering Science vol. 235.2, 2021, pp. 461-470.

[13] M. Zhao, T. Barber, P. Cistulli, K. Sutherland, G. Rosengarten, Computational fluid dynamics for the assessment of upper airway response to oral appliance treatment in obstructive sleep apnea, Journal of biomechanics vol. 46.1, 2013, pp. 142-150.

[14] A. Ibbeken, C. Hagen, F. Zell, A. Steffen, Ulrike Grzyska, A. Frydrychowicz, T. M. Buzug, Design and construction of a flexible pharyngeal phantom, Transactions on Additive Manufacturing Meets Medicine vol. 3(1), 2021, pp. 499.

[15] P.A. Yushkevich, J. Piven, H.C. Hazlett, R.G. Smith, S. Ho, J.C. Gee, G. Gerig, User-guided 3D active contour segmentation of anatomical structures: Significantly improved efficiency and reliability, Neuroimage vol. 31.3, 2006, pp. 1116-1128.

[16] A. Malhotra, Y. Huang, R.B. Fogel, G. Pillar, J.K. Edwards, R. Kikinis, S.H. Loring, D.P. White, The Male Predisposition to Pharyngeal Collapse Importance of Airway Length, American Journal of Respiratory and Critical Care Medicine, vol. 166, 2002, pp. 1388-1395.

[17] S. Cheng, S.C. Gandecia, M. Green, R. Sinkus, L.E. Bilston, Viscoelastic properties of the tongue and soft palate using MR elastography, Journal of Biomechanics vol. 44.3, 2011, pp. 450-454.

[18] R. N. Palchelsko, L. Zhang, Y. Sun, A.W. Feinberg, Development of Polydimethylsiloxane substrates with Tunable Elastic Modulus to Study Cell Mechanobiology in Muscle and Nerve, PLoS ONE vol. 7.12, 2012, pp. e51499.

[19] R. L. Owens, B. A. Edwards, S. A. Sands, J. P. Butler, D. J. Eckert, D. P. White, A. Malhotra, A. Wellman, Upper airway collapsibility and patterns of flow limitation at constant end-expiratory lung volume, Journal of applied physiology vol. 113.5, 2012, pp. 691-699.

[20] E. Kazemeini, E. Van de Perck, M. Dieltjens, M. Willemen, J. Verbraecken, S. Op de Beeck, O.M. Vanderveken, Critical to Know Pcrit: A Review on Pharyngeal Critical Closing Pressure in Obstructive Sleep Apnea, Frontiers in neurology vol. 13: 775709, 2022.